有限要素法에 의한 V溝JFET의 解析에 관한 硏究

論 文
30～10～2

A Study on the Analysis of a Vertical V-groove Junction Field Effect Transistor with Finite Element Method

成 英 權* · 成 萬 永** · 金 一 洙*** · 朴 贊 元***
(Yung-Kwon Sung·Man-Young Sung·Il-Soo Kim·Chan-Won Park)

Abstract

A technique has been proposed for fabricating a submicron channel vertical V-groove JFET using standard photolithography.

A finite element mumerical simulation of the vertical V-groove JFET operation was performed using a FORTRAN program run on a Cyber-174 computer. The numerical simulation predicts pentode like common source output characteristics for the p^+n Vertical V-groove JFET with maximum transconductance representing approximately 6 precent of the zero bias drain conductance value and markedly high drain conductance at large drain voltages. An increase in the acceptor concentration of the V-groove JFET gate was observed to cause a significant increase in the transconductance of the device. Therefore, as above mentioned, this paper is study on the analysis of a Vertical V-groove Junction Field Effect Transistor with Finite Element Method.

1. Introduction

The finite element method[1][2] has been developed in mechanical engineering and civil engineering, as a numerical analysis technique for large scale frames. This method is a kind of direct method based on the variational principle. By partitioning the continuum, which has an infinite degree of freedom, into elements interconnected at a finite number of nodal points, this method has been applied to continuous materials as well as discrete ones. In addition, when the variational principle does not hold, namely, it does not give a functional corresponding to a given partial differential equation, it can be formulated by the method of weighted residuals[2], similar to the finite-element method. In this way, the finite element method becomes applicable in several fields of engineering. In electrical engineering, this method is also applied for analysis of an electromagnetic field in a waveguide, and so on. Recently, two-dimensional analysis of semiconductor devices by this method has been reported.[3][4] In this method, a large scale matrix is formed in a grid like mesh, so an iterative method is used. It also has the little flexibility for parameter dependence and geometry irregularity.

On the other hand, in a finite element method, the objectives can be partitioned arbitrarily. Then, local element refinement can be achieved, in rapid change regions. In slow change regions it can be divided into coarse elements. For this reason the total number of nodes reduced in this method, but the structure of obtained matrix becomes complicated and then the bandwidth of this matrix will increase. Thus to save on memory storage requirements and to reduce computing time, a

* 正會員 : 高麗大 工大 電氣工學科 敎授 · 工博
** 正會員 : 檀國大 工大 電氣工學科 助敎授 · 工博
*** 正會員 : 高麗大 大學院 電氣工學科 碩士課程
接受日字 : 1981年 7月 15日

matrix reordering algorithm is introduced. It is easy to treat an arbitrary geometry and to set up parameters elements by element. The main advantage of this method is that the current conservation law is always satisfied if the solution converges, without regard for a coarse approximation, not only at terminals but also within closed regions. Furthermore, total charge calculation is comparatively accurate at a coarse approximation. In this paper, a new vertical V-groove JFET structure[5][6] is proposed which is expected to achieve useful high frequency characteristics. To better understand the principles of operation of the proposed vertical V-groove JFET, a two-dimensional numerical simulation of the JFET structure is performed for various conditions. Therefore, the methods and results of a two-dimensional finite element simulation of vertical V-groove JFET are presented. And the simulation is used to determine the output characteristics and transconductances as well as the two dimensional distributions of voltage, electron density and electric field for the vertical V-groove JFET. The following sections give details on finite element formulation of two dimensional V-groove JFET structure and resulting calculation.

2. Proposed Vertical V-groove Junction Field Effect Transistor[5][6][15][16]

A vertical V-groove JFET structure is proposed in this paper which expected to achieve useful power gain in high frequencies. A cross-sectional diagram of the proposed vertica V-groove JFET

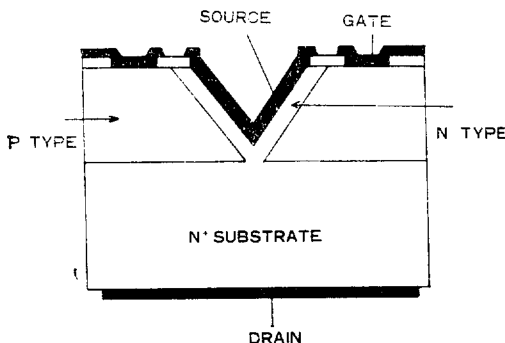

Fig. 1. Proposed vertical V-groove JFET structure

is shown in Fig. 1. This device is expected to have the following advantages over previously proposed JFET structures.

1) A submicron channel will be fabricated utilizing standard photolithographic techniques without requiring excessively small mask dimensions.

2) Electron mobility in the channel will be high due to the low doping levels used.

3) Parasitic source resistance will be greatly reduced.

To better understand the principles of operation of the proposed vertical V-groove JFET, a two dimensional numerical simulation of the vertical V-groove JFET structure was performed for various bias conditions. The simulation program[1][2] utilized the finite element method for analyzing time-dependent partial differential equations with boundary and initial conditions.

3. Finite Element Representation of Semiconductor Device Equations[3][4][6][7]

The particular equations to be solved for the vertical V-groove JFET structure and Poisson's equation,

$$\nabla^2 V=\frac{q}{\varepsilon}(n-p-N_D+N_A) \tag{1}$$

and the continuity equations for electrons and holes, respectively,

$$\frac{\partial n}{\partial t}=\nabla\cdot(J_n/q)+G_n-R_n \tag{2}$$

and

$$\frac{\partial p}{\partial t}=-\nabla\cdot(J_p/q)+G_p-R_p \tag{3}$$

where

$$J_n/q=-nV_n+D_n\nabla n \tag{4}$$

$$J_p/q=PV_p-D_p\nabla P \tag{5}$$

n ; electron concentration

p ; hole concentration

D_n, D_p ; electron-and hole diffusion coefficients, respectively

V_n, V_p ; electron-and hole velocity vectors, respectively

Equation (1)—(3) can be simplified by assuming

that (i) minority carriers can be neglected everywhere in the device and (ii) generation (G_n, G_p) and recombination (R_n, R_p) can be neglected for majority carriers everywhere in the device. Under these assumptions, *Eqs* (1)—(3) can be written separately on the n-side of the junction as

$$\nabla^2 V = \frac{q}{\varepsilon}(n - N_D) \qquad (6)$$

$$\frac{\partial n}{\partial t} = \nabla \cdot (J_n/q) \qquad (7)$$

and on the p-side of the junction as

$$\nabla^2 V = -\frac{q}{\varepsilon}(p - N_A) \qquad (8)$$

$$\frac{\partial p}{\partial t} = -\nabla \cdot (J_p/q) \qquad (9)$$

The finite element method will be described here briefly as it relates to the solution of *Eqs*(6)~(9).

Let $U(\chi)$ be the solution vector of a set of two dimensional partial differential equations over region D with appropriate boundary and initial conditions; thus U must satisfy the equation

$$A[U] = 0 \qquad (10)$$

where A is a nonlinear operator and χ equals (x, y). If $\bar{U}(\chi)$ is an approximation function to U, then the residual of U is defined by

$$R = A[\bar{U}] \qquad (11)$$

Clearly if $R=0$, then $\bar{U}$ is an exact solution of *Eq.* (10). A approximate solution of *Eq.* (10) can be found by assuming that R be orthogonal to each of a weighting functions $\{W_i\}$ $i=1, 2, 3, \cdots\cdots N$, over the region D,

$$\int_D W_i R dS = 0, \quad i=1, 2, \cdots\cdots N \qquad (12)$$

where N is equal to the number of adjustable parameters in $\bar{U}$. Next let a mesh be superimposed over the region D dividing it into smaller regions called elements. Associated parameter with each element is a number of nodes on its boundary. The approximating function $\bar{U}$ can be represented within each element e by

$$U = \sum_i \bar{U}_i f_i^e(\chi) \qquad (13)$$

where $\bar{U}_i$ is the value of U at node i and $f_i^e(\chi)$ is an element shape function associated with node i which satisfies the condition

$$f_i^e(\chi_j) = \begin{cases} 1 & i=j \\ 0 & i \neq j, \ i, j \text{ in } e \end{cases} \qquad (14)$$

where χ_j is the vector representation of he coordinates of node j. The summation is over all nodes in element e. By extending the definition of the element shape functions to be identically zero everywhere outside of element e, the summation in *Eq.* (13) can be adjust to extend from 1 to N, where N is now the number of nodes in region D less the number of nodes on conducting boundaries.

On the other hand, the residual for element e can be found by substituting *Eq.* (13) into *Eq.* (11) thus giving

$$R_e = A[\sum_{i=1}^{N} \bar{U}_i f_i^e] \qquad (15)$$

The weighting function [2] W_j can be chosen in any of a number of ways. For this analysis a weighting function is defined for each node j according to

$$W_j = \sum_{e(j)} f_j^e, \quad j=1, 2, \cdots N., \qquad (16)$$

where the notation $\sum_{e(j)}$ denotes a summation over all elements containing node j. In elements which do not contain node j, $W_j=0$. This choice for W_j is know as Galerkin's method.[2] The weighting functions so defined are called "hill"[8] function due to their shape (see Fig. 2). The orthogonality condition (E_q. 12) can now be written as

$$\sum_{e(j)} \int_{D_e} R_e f_j^e \, dS = 0, \quad j=1, 2 \cdots\cdots N \qquad (17)$$

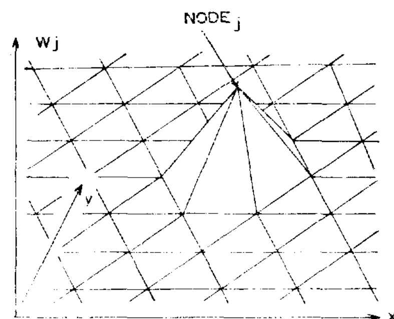

Fig. 2. "Hill" function $W_j(\chi)$ for triangular mesh with linear shape functions $f_j^e(\chi)$

Using the finite element method, and algorithm for determining voltage and majority carrier

distributions over the predescribed region D can now be developed. Consider first Poisson's equation

$$\nabla^2 V = -\frac{\rho}{\varepsilon}$$

where

$$\rho = \begin{cases} -q(n-N_D) & \text{on the } n\text{-side of the junction} \\ q(p-N_A) & \text{on the } p\text{-side of the junction} \end{cases}$$

In the notation developed above, the solution vector U is simply the voltage $V(\chi)$. Then Eq (10) becomes

$$A[U] = \nabla^2 V + \frac{\rho}{\varepsilon} = 0 \tag{18}$$

The residual is

$$R = \nabla^2 \bar{V} + \frac{\bar{\rho}}{\varepsilon} \tag{19}$$

where $\bar{V}(\chi)$ and $\bar{\rho}(\chi)$ are the approximating functions to $V(\chi)$ and $\rho(\chi)$, respectively.

Within any element e, the quantity $\int_{D_e} R_e f_j^e dS$ from $Eq.$ (17) can be written as

$$\int_{D_e} R_e f_j^e dS = \int_{D_e}\left[\nabla^2 \bar{V} + \frac{\rho}{\varepsilon}\right] f_j^e dS = -\int_{D_e}\left[(\nabla \bar{V} \cdot \nabla f_j^e) - \left(\frac{\rho}{\varepsilon}\right) f_j^e\right] dS \tag{20}$$

where, on nonconducting boundaries, the normal component of $\nabla \bar{V}$ is idenitcally zero (Neumann boundary condition). Now let the approximating functions for the voltage $\bar{V}$ and the space charge ρ within each element e, be written as

$$\bar{V} = \sum_{i=1}^{N} V_i f_i^e \tag{21}$$

and

$$\rho = \sum_{i=1}^{N} \rho_i f_i^e \tag{22}$$

Substituting Eqs (20)~(22) into Eq (17), it is found that

$$\sum_{e(j)} \int_{D_e} \left[\sum_{i=1}^{N} V_i \nabla f_i^e \cdot \nabla f_j^e - \frac{\rho_i}{\varepsilon} f_i^e f_j^e\right] dS = 0 \tag{23}$$

$$j = 1, 2, \cdots\cdots N$$

Interchanging summations and rearranging,

$$\sum_{i=1}^{N}\left[K_{ji}{}^{V} V_i - M_{ji}{}^{V} \frac{\rho_i}{\varepsilon} = 0, \quad j = 1, 2 \cdots\cdots N \tag{24}\right.$$

where

$$K_{ji}{}^{V} = \sum_{e(j)} \int_{D_e} \nabla f_i^e \cdot \nabla f_j^e \, dS \tag{25}$$

$$M_{ji}{}^{V} = \sum_{e(j)} \int_{D_e} f_i^e f_j^e dS \tag{26}$$

$Eq.$ (24) is an $N \times N$ matrix equation for the N unknowns V_i. When values of the space charge ρ_i are known and appropriate element shape functions f_i^e have been chosen, this equation can be solved using sparse matrix techniques[9] or interative technique to find $\{V_i\}$.

The electron and hole continuity equations ($Eq.$ (7), (9)) can be solved in a similar fashion. In the case of Eq (7), the solution vector is $n(\chi)$ and the residual is

$$R = \frac{\partial \bar{n}}{\partial t} - \nabla \cdot (-n V_n + D_n \nabla \bar{n}) \tag{27}$$

The electron drift velocity V_n is assumed constant within an element. Equation (27) then becomes

$$R = \frac{\partial \bar{n}}{\partial t} + V_n \nabla \bar{n} - D_n \nabla^2 \bar{n} \tag{28}$$

Then the term $\int_{D_e} R_e f_j^e dS$ in Eq (17) can be written as

$$\int_{D_e} R_e f_j^e \, dS = \int_{D_e}\left[\frac{\partial \bar{n}}{\partial t} f_j^e + V_n \nabla \bar{n} f_j^e + D_n \nabla \bar{n} \cdot \nabla f_j^e\right] dS \tag{29}$$

An expression for the electron concentration $\bar{n}$ can be written similar to $Eq.$ (21).

$$\bar{n} = \sum_{i=1}^{N'} \bar{n}_i f_i^e \tag{30}$$

where N' is the number of interior and nonconducting boundary nodes in D at which electrons predominates.

Substituting $Eq.$ (21), (29) and (30) into $Eq.$ (17), it is found that

$$\sum_{e(j)} \int_{D_e} \sum_{i=1}^{N'}\left[\frac{\partial \bar{n}_i}{\partial t} f_i^e f_j^e + \bar{n}_i \cdot V_n \cdot \nabla f_i^e f_j^e + D_n \bar{n}_i \nabla f_i^e \cdot \nabla f_j^e\right] dS = 0, \quad j = 1, 2, 3, \cdots\cdots N' \tag{31}$$

In order to include the time evolution of the electron concentration $\frac{\partial \bar{n}_i}{\partial t}$ in the above equations, the value of $\bar{n}_i$ after K time steps is designated $\bar{n}_i^K$. Then

$$\frac{\partial \bar{n}_i}{\partial t} = \frac{\bar{n}_i^{K+1} - \bar{n}_i^K}{\Delta t} \tag{32}$$

where Δt is the value of the time step. For all other occurrence of $\bar{n}_i$ in Eq (31)

$$\bar{n}_i = \theta \bar{n}_i^{K+1} + (1-\theta) \bar{n}_i^K \tag{33}$$

where

$$0 \leqq \theta \leqq 1 \tag{34}$$

when $\theta = 0$ the term $\bar{n}_i^{K+1}$ appears only in the time-derivative term(Eq 32). The time evolution scheme for this case is said to be explicit.[3][6][10] Similarly when $\theta = 1$, the time evolution scheme is

called implicit.[3][6][10]

In this analysis θ is chosen as 0.5.

Now, Substituting *Eq.* (32) and (33) into (31) gives

$$\sum_{e(j)}\int_{De}\sum_{i=1}^{N'}\left\{\frac{\bar{n}_i^{K+1}-\bar{n}_i^K}{\Delta t}f_i^e f_i^e+[\theta\bar{n}_i^{K+1}+(1-\theta)\bar{n}_i^K]\right.$$
$$\left.[V_n\nabla f_i^e f_j^e+D_n\nabla f_i^e\cdot\nabla f_j^e]\right\}dS=0,\quad j=1,2,\cdots\cdots N' \quad (35)$$

Interchanging summation and rearranging

$$\sum_{i=1}^{N'}\{M_{ji}^V+\theta\Delta t\ [B_{ji}^C+D_nK_{ji}^V]\bar{n}_i^{K+1}-[M_{ji}^V$$
$$-(1-\theta)\Delta t\ (B_{ji}^C+D_nK_{ji}^V)]\bar{n}_i^K\}$$
$$=0,\quad j=1,2,\cdots\cdots N' \quad (36)$$

where

$$B_{ji}^C=\sum_{e(j)}\int_{De}V_n\cdot\nabla f_i^e f_j^e\ dS \quad (37)$$

and K_{ji}^V and M_{ji}^V are defined by *Eq.* (25) and (26), respectively.

Equation (36) is an $N'\times N'$ matrix equation in the N' unknowns $\{\bar{n}_i^{K+1}\}$ When values of $\bar{n}_i^K$ and V_n have been determined and $\theta, \Delta t$ and the element shape functions f_i^e have been chosen appropriately, *Eq* (36) can be solved for the electron concentration $\{\bar{n}_i^{K+1}\}$.

An equation similar to *Eq* (36) can be set up for the nodes on the p-side of the junction. This equation can be solved to find $\{\bar{p}_i^{K+1}\}$ to complete the approximating function for the majority carrier distribution in region D. FORTRAN computer program has been written which formulates Poisson's equation and the majority carrier continuity equations in terms of their finite element representations and then solves alternately for the voltage and carrier concentration approximating functions over a specified number of time steps with a flow chart of Fig. 3.

The element shape functions chosen for this analysis are simpl ylinear function of theform,[6][7]

$$f_i^e=(\alpha_1+\alpha_2x+\alpha_3y)/2\Delta \quad (38)$$

where α_1, α_2 and α_3 are constants, and Δ is the area of triangular element.

In order to use the finite element numerical technique described above to analyze the proposed vertical V-groove JFET structure, a two dimensional model of the interior of the device must be constructed with an appropriate grid overlay. The model chosen for this analysis is shown in Fig. 4. A regular grid overlay consisting of isosceles triangles with height 0.092μm and base 0.13μm was superimposed over the model.

On the other hand, as with any numerical technique for solving time-dependent partial differential

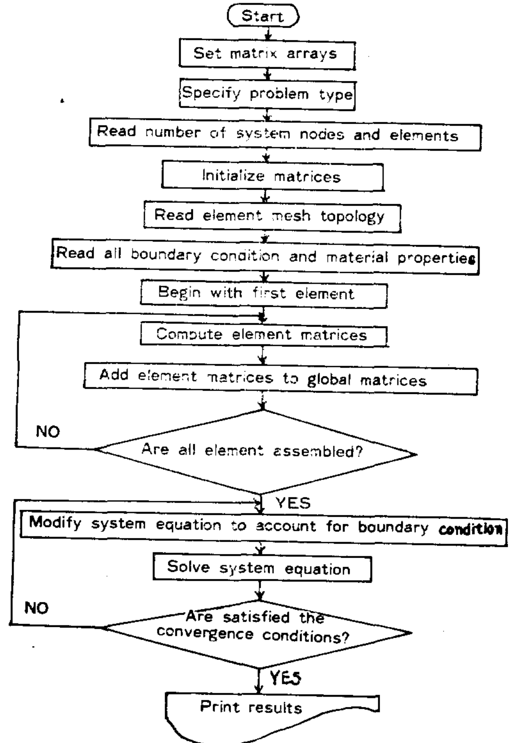

Fig. 3. Flow chart for a computer program to solve steady state vertical V-groove JFET characteristics problem by the finite element method

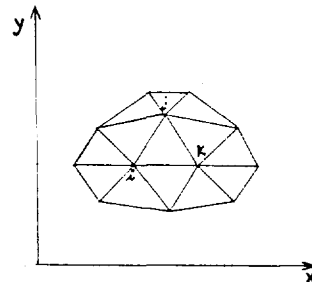

Fig. 4. Isosceles triangular elements with height 0.092μm and base 0.13μm

equations, some restrictions exist on the choices for serveral of the parameters of the finite element method in order to guarantee that the approximating functions obtained will converge on a valid solution of the original equations.

The dielectric relaxation time given by ε/σ represents the constraint on the time step. The material conductivity can be expressed as

$$\sigma=q(\mu_p p+\mu_n n) \tag{39}$$

Since the V-groove JFET is a majority carrier device, this stability condition[3][4] can be written as

$$\Delta t \leqq \left[\frac{\varepsilon}{q\mu_p p} \text{ or } \frac{\varepsilon}{q\mu_n n}\right] \tag{40}$$

Violation of this condition can result in instabilities either in space charge or in electric feld.

4. Analysis of p⁺n vertical V-groove JFET

4.1 Two dimensional p⁺n vertical V-groove JFET model

The mathematical basis for the finite-element analysis of the proposed vertical V-groove JFET structure has been presented and discussed. Using the simulation program to study the operation of the p⁺n vertical V-groove JFET with equal impurity concentrations on each side of junction, it was observed that very high values of drain current with very low associated values of transconductance were obtained. The cause of this behavior was traced to two mechanisms. First the curvature in the p n junction near the drain end of the channel forced the largest fraction of the depletion region to lie in the p-type gate rather than extending equally into the gate and n-type channel. This caused a greater current to flow in the channel for a given drain bias than would be expected from the simple theory of operation. Additionally, the excess electrons had the effect of increasing the conductivity of the channel while reducing the transconductance of the V-groove JFET by preventing the movement of the depletion layer edge into channel and tunneling between the channel and t he drain.

The low transconductance and high output conductance exhibited by the pn vertical V-groove JFET can be significantly improved by increasing the doping in the gate region while maintaining a relatively light doping level in the channel. The effect of the p⁺n structure will be to force the depletion region into the channel, thereby minimizing the rounding of the channel and the tunneling effect at the drain end. An applied gate voltage will then modulate the channel width much more effectively than in the case of the pn vertical V-groove JFET.

The model used for the two dimensional numerical simulation of the p⁺n vertical V-groove JFET is shown in Fig. 5. A doping level of $N_A=1.0\times10^{18}\text{cm}^{-3}$ was assumed in the p-type gate with $N_D=5.0\times10^{15}\text{cm}^{-3}$ in the n-type channel. The doping near the source and drain was again assumed to be $N_D=1.0\times10^{16}\text{cm}^{-3}$ to simulate ohmic contact regions.

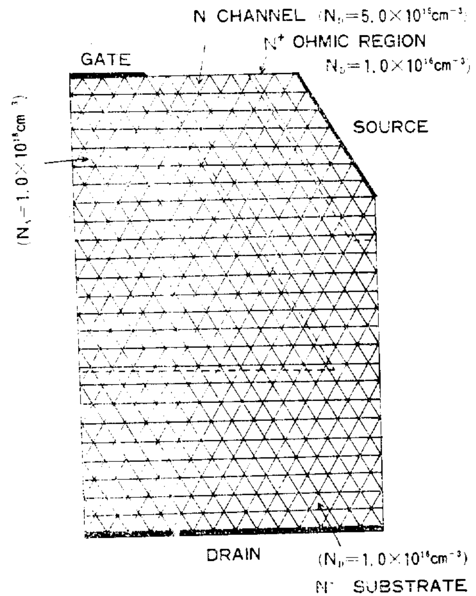

Fig. 5. Model of vertical p⁺n V-groove JFET for numerical analysis.

The electrical behavior of the vertical p⁺n V-groove JFET will be determind solely by the distribution and transport properties of electrons on the lightly doped side of the junction due to the very high relative doping in the gate region. The analysis of this structure was therefore

restricted to a majority carrier simulation in the n-type regions of the device. The gate terminal was located at the metallurgical p^+n junction. This placement is reasonable only if the highly doped p-region can be considered as an equipotential and if the depletion width on the p-side of the junction can be neglected.

The boundary conditions on electron concentration at the gate nodes are assumed to be the following.

Dirichlet boundary conditions[4][6][10] were assumed for all conduction boundaries, i,e., for Poisson's equation,

$$V=\begin{cases} 0 & \text{at all source nodes} \\ V_G & \text{at all gate nodes} \\ V_D & \text{at all drain nodes} \end{cases}$$

and for the continuity equations,

$n=1\times10^{16}\text{cm}^{-3}$ at all source and drain nodes, and $p=1\times10^{18}\ \text{cm}^{-3}$ at all gate nodes. At all other boundary nodes, Neumann conditions[4][6][10] were assumed so that for Poisson's equation

$$\nabla V\cdot \hat{n}=0 \tag{41}$$

at all non-conducting boundary nodes, and for the continuity equation

$$\nabla n\cdot \hat{n}=0 \tag{42}$$

at all n-type non-conducting boundary nodes, and

$$\nabla p\cdot \hat{n}=0 \tag{43}$$

at all p-type non-conducting boundary nodes, where $\hat{n}$ represents the normal unit vector.

For the first program run(corresponding to given value of V_G and V_D), the initial conditions on n and p at each node in the model were chosen as

$$n=N_D \tag{44}$$

$$p=N_A \tag{45}$$

For all successive runs, initial conditions on n were chosen as the final values from the previous run. A velocity vs electric field relationship[6][10] of the form was assumed for electrons

$$V_n=-\frac{\mu_{n0}E}{1+\frac{\mu_{n0}|E|}{V_{nsat}}} \tag{46}$$

and

$$V_p=\frac{\mu_{p0}E}{1+\frac{\mu_{p0}|E|}{V_{psat}}} \tag{47}$$

for holes where $\mu_{n0}=1,200\text{cm}^2/V\text{-}S$, $\mu_{p0}=400\text{cm}^2/V\text{-}S$ and $V_{nsat}=V_{psat}=1\times10^7\text{cm/s}$. Electron and hole diffusion coefficients D_n and D_p were assumed to be independent of electric field with values of $31.1\text{cm}^2/\text{s}$ and $10.4\text{cm}^2/\text{s}$, respectively. A time step of $\Delta t=5\times10^{-13}$ was selected. The built-in voltage was assumed to be 0.8V. Convergence of the simulation to a steady-state condition was assumed to occur whenever the maximum change in voltage at any node was less than 0.009V per time step, the maximum change in electron concentration at any node was less than $1.0\times10^{14}\text{cm}^{-3}$ per time step.

4.2 DC Output Characteristics

Figure 6 and 7 represent the electron concentration profiles with no gate bias applied and $V_D=0.5$ and 2.5, respectively. The increasing electron concentration in the channel is clearly apparent from these figures. The excess charge in the channel also has the effect of preventing the output current from saturating.

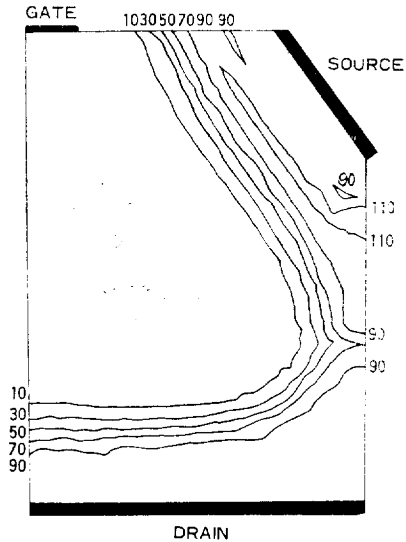

Fig. 6. Electron concentration contours for p^+n vertical V-groove JFET ($V_D=0.5V$, $V_G=0$)

The increase in excess electron region with drain voltage inhibits the spreading of the depletion into the channel as well as adding an excess component to the drain current.

Figure 8 is an electric field profiles of the p^+n vertical V-groove JFET structure when $V_D=0.5\text{V}$ and $V_G=0$. From this profile it can be seen that the electric field in the channel is below the value necessary to saturate electron velocities at their

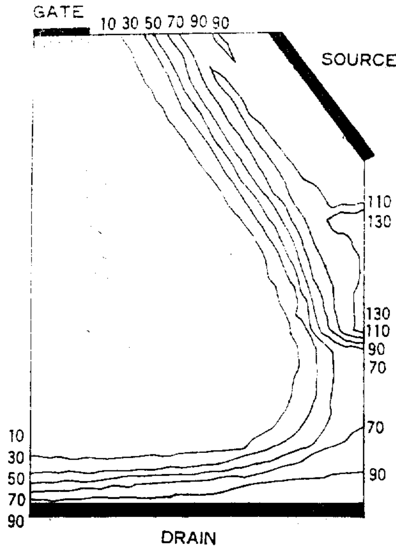

Fig. 7. Electron concentration contours for p⁺n vertical V-groove JFET($V_D=2.5V$, $V_G=0$)

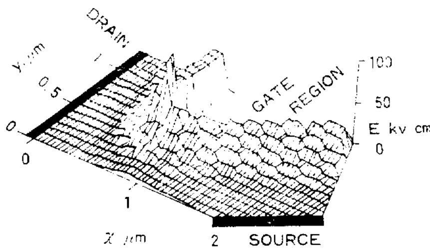

Fig. 8. Electric field distribution in p⁺n vertical V-groove JFET ($V_D=0.5V$, $V_G=0$)

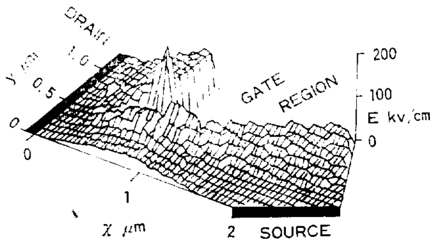

Fig. 9. Electric field distribution in p⁺n vertical V-groove JFET ($V_D=2.5V$, $V_G=-1.0V$)

scattering-limited value of 1.0×10^7cm/s. The same field profile when $V_D=2.5$V and $V_G=-1.0$V is shown in Fig. 9.

As expected, field values everywhere in the structure are much larger for this case. In particular, the electric field at many points in the channel is large enough to cause electrons to reach their scattering-limited velocities. Thus the JFET operation will be dominated by hot electron effects for moderate terminal voltages. The simplification used for the long channel JFET cannot be used in the analysis of the vertical V-groove JFET. To a good approximation, it is found that the onset of determined breakdown in an abrupt pn junction is avalanche by the maximum electric field in the depletion region.

The dashed lines of Fig. 10 represent total drain current for several values of V_G as predicted by the numerical simulation. These data are compared to an approximate mathematical expression for the p⁺n junction output characteristics based on the simple one dimensional model.

In order to evaluate the results of the numerical simulation it is necessary to make an approximate analysis of the JFET structure. It shall be assumed that the output characteristics[11] takes the form

$$I_D=\frac{g_0V_p}{1+\frac{\mu_0V_D}{v_{sath}}}\left\{\frac{V_D}{V_p}-\frac{2}{3}\left[\left(\frac{V_D-V_G+V_{bi}}{V_p}\right)^{3/2}\left(\frac{-V_G+V_{bi}}{V_p}\right)^{3/2}\right]\right\} \tag{48}$$

where g_0 is the channel conductance with no depletion layer formed, V_p is the pinch-off voltage of an abrupt junction JFET, and all other symbols take their usual meanings.

From $Ep.$ (48)

$$g_m=\frac{g_0}{1+\frac{\mu_0V_D}{v_{sat}L}}\left[\left(\frac{V_D-V_G+V_{bi}}{V_p}\right)^{1/2}-\left(\frac{-V_G+V_{bi}}{V_p}\right)^{1/2}\right] \tag{49}$$

$$g_d=\frac{g_0}{1+\frac{\mu_0V_D}{v_{sat}L}}\left[1-\left(\frac{V_D-V_G+V_{bi}}{V_p}\right)^{1/2}\right]-\frac{\mu_0I_D}{v_{sat}L+\mu_0V_D} \tag{50}$$

for $V_D-V_G+V_{bi}<V_p$. For all $V_D-V_G+V_{bi}\geqq V_p$, g_d is assumed to equal zero and g_m is assumed to maintain a constant value. The solid curves of Fig. 10 are again assumed to be of the form of Eq(48) where V_p is now pinch-off voltage ($V_p=3.2$V) at the drain of the p⁺n V-groove JFET.

Values of output conductance g_d and transconductance g_m for the simulated JFET were calculated

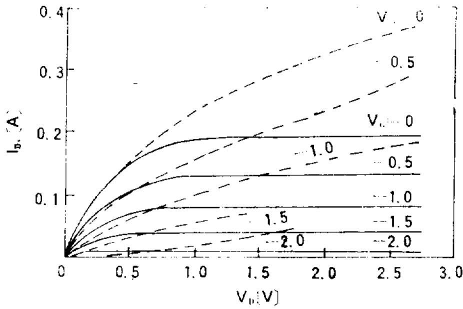

Fig. 10. Vertical p^+n V-groove JFET output characteristics from numerical analysis (dashed lines) and from theoretical analysis (solid lines)

from data of Fig. 10 and are plotted as dashed lines in Fig. 11. These values are compared to transconductance and outputconductance values found from *Eqs* (49) and (50), respectively. In the saturation region, g_d is assumed to be zero, while g_{msat} is found from the saturated portions of the curves in Fig. 10. The transconductance is shown in Fig. 11 for $V_G=-0.25$V. The output conductance is plotted for $V_G=0$.

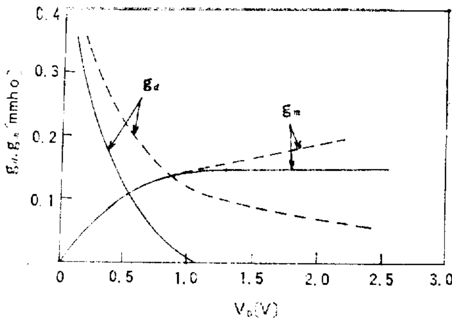

Fig. 11. p^+n vertical V-groove JFET output conductance g_d ($V_G=0$) and transconductance g_m ($V_G=-0.25$V) from numerical analysis (dashed lines) and from theoretical analysis (solid lines)

At low values of drain voltage, the agreement between currents found from the numerical simulation and those calculated from *Eq* (48) is excellent However as the drain voltage increases the resultant drain current attains much higher values than *Eq.* (48) predicts. As in the case of the pn vertical V-groove JFET, this excess current can be attributed to the formation of excess electron region in the channel. Hence, the output current increases with drain voltage for all values of gate voltage rather than saturating as the simple model predicts. The output conductance therefore shows good agreement with *Eq.* (50) at low values of V_D before the excess current becomes significant, but remains consistently larger than zero in the saturated region of the output characteristics.

The transconductance is also strongly affected by the excess electron in the channel. From Fig. 11, it is readily apparent that the transconductance agrees with *Eq* (49) for small V_D, but is even greater than the calculated g_{msat} for larger drain voltages. This increase is directly attributable to the excess carrier in the channel. More charge must be removed from excess carrier regions than from the neutral channel in order to extend the depletion region. An applied gate voltage will therefore moduate the excess current in addition to the normal conduction current, thereby enhancing the transconductance.

It must therefore be concluded that the mechanism preventing current saturation in the vertical V-groove JFET is simply the excess electrons and tunneling effects in the channel.

5. Conclusions

The methematical basis for the finite element analysis of the proposed vertical V-groove JFET structure has been presented and discussed. Using the simulation program to study the operation of p^+n vertical V-groove JFET with p^+n impurity concentrations on the junction, it was observed that very high values of drain current with very low associated values of transconductance were obtained. The cause of this behavior was tracted two mechanisms. First the curvature in the V-groove near the drain end of channel forced the largest fraction of the depletion region to lie in the p^+ type gate rather than extending into the n-type channel. This caused a greater current to flow in the channel for a given drain bias than would be expected from the horizontal V-groove FET of F.E. Holmes.[12] Additionally, the excess

electrons regions had the effect of increasing the conductivity of the channel while reducing the transconductance of vertical V-groove JFET by preventing the movement of depletion layer edge into the channel.

Specially, the simulation program was then used to study the V-groove JFET with the gate acceptor doping level increased to a very high value. The large acceptor concentration had the effect of forcing the depletion region into the channel when a gate bias was applied. The excess electron concentration in the channel could now be modulated by an applied gate voltage, resulting in higher transconductance values than Neumark and Rittner's JFET theory[11] predicted. However, the excess electron region in the channel was again found to cause a high output conductance for large values of drain bias.

Reference

〔1〕 Kenneth H. Huebner; "The finite element method for engineers", John Wiley & Sons, Inc. 1975.

〔2〕 Edward L Wilson; "Numerical method in finite element analysis", Prentice-Hall, Inc. 1976.

〔3〕 Tohru Adachi. "Two dimensional semiconductor analys is using finite element method", IEEE Trans. Electron Devices vol. 26, No. 7, pp. 1026~1030, 1979.

〔4〕 J.J. Barnes; "Two dimensional finite element simulation of semiconductor device", Electronics Letters vol. 10, No. 16, pp. 341~343, 1974.

〔5〕 M.Y. Sung and Y.K. Sung; "A study on the experimental fabrication and analysises of the new field effect transistor", J. KEES. 1980. 4.

〔6〕 M.Y. Sung; "A evaluation on the impurity concentration of V-FET", J. KIEE. 1980. 11.

〔7〕 John J. Barnes; "Finite element simulation of GaAs MESFET's with lateral doping profiles and submicron gates", IEEE Trans. Electron Devices, vol. 23, No. 9, 1042, 1976.

〔8〕 Pipes and Harvill; "Applied mathmatics for engineers and physicists", MaGraw-Hill 1970.

〔9〕 H.A. Luther; "Applied numerical methods", John Wiley & Sons Inc. 1969.

〔10〕 R.J. Lomax; "Transient two-dimensional simulation of a submicrometer gate-length MESFET", Electronics Letters vol. 11, No. 1, pp. 519~521, 1975.

〔11〕 Richard S. Cobbold; "Theory and applications of field effect transistors", Wiley-interscience, 1970.

〔12〕 F.E. Holmes; "VMOS-A New MOS integrated circuit technology", Solid state electronics vol 17, pp. 791~797, 1974.

〔13〕 Martin Resier; "A Two-dimensional numerical FET model for DC, AC and large signal anslysis", IEEE Trans. Electron Devices, vol. 20, No. 1 pp. 35~45, 1973.

〔14〕 Donald C. Mayer; "A vertical-junction field effect Tr", IEEE Trans. Electron Devices vol ED-26 pp. 956~961, May. 1980.

〔15〕 M.Y. Sung; V-groove vertical channel field effect transistor", IDRC Report 1977, No. N00014—77—C—0418

〔16〕 M.Y. Sung; "A study on the experimental fabrication and analysis of the diffusion self aligned V-groove FET for high speed devices", Dissertation, September, 1977.

〔17〕 IDRC, Sung. M.Y.; "V-groove vertical channel field effect transistor", US Patent. Application No. 883588